

Experimental demonstration of three-photon Coherent Population Trapping in an ion cloud

M. Collombon, C. Chatou, G. Hagel, J. Pedregosa-Gutierrez, M. Houssin, M. Knoop, and C. Champenois*

Aix Marseille Univ, CNRS, PIIM, Marseille, France

(Dated: July 17, 2019)

A novel protocol of interrogation based on coherent population trapping in an N -level scheme atomic system leads to dark resonances involving three different photons. An ensemble of several hundreds of radio-frequency trapped Ca^+ ions is probed by three lasers simultaneously locked onto the same optical frequency comb, resulting in high-contrast spectral lines referenced to an atomic transition in the THz domain. We discuss the cause of uncertainties and limitations for this method and show that reaching a sub-kHz resolution is experimentally accessible via this interrogation protocol.

PACS numbers:

The quantum interferences between two excitation paths which are responsible for coherent population trapping (CPT) are an example of a quantum effect based on atomic coherences [1]. When this interference occurs in a Λ -scheme atomic system, the atomic population is trapped in a coherent superposition of the two ground sub-states, dressed by the coupling photons. If the two ground dressed sub-states are stable, the excited state is no more populated. This population trapping can be observed by a dark resonance in the fluorescence signal [2] or by the cancellation of the laser absorption [3]. Two-photon CPT has proven its relevance as a resource for high precision measurement in magnetometry [4, 5] and in the so-called "CPT-microwave clock" where no microwave cavity is needed anymore [6–8]. The best reported performances concerning short term stability are reached with vapour cell clock with fractional frequency stability of few $10^{-13}/\sqrt{\tau}$ [9, 10]. Cold atom clocks are expected to perform better regarding long term stability and an instability of the order of 3×10^{-13} after one hour of averaging time is reported in [11]. In this paper, we report the observation of a three-photon CPT in a cold cloud of trapped ions and discuss its main causes of shift and broadening.

In CPT-microwave clocks, two phase-coherent lasers perform optical spectroscopy of the GHz-transition between hyperfine sub-levels of the heaviest alkalis Rb and Cs. When the laser difference frequency matches the ground-state splitting, the atomic population is trapped in a dark state and the optical signal is used to reference this frequency difference to the GHz-transition. Sub-Doppler spectroscopy is reached by exploiting the Lamb-Dicke effect [12] which provides a first-order Doppler cancellation whenever the displacement of the absorbers over successive excitation is smaller than $\lambda/(2\pi)$ with λ the transition wavelength, of the order of centimeters for microwave transition and micrometers for optical transi-

tions. Experimental results in room temperature cells where the atom mean-free-path is reduced to millimeter scale by filling with buffer gas or by scaling the cell size to millimeter prove that the Lamb-Dicke regime can be reached for the microwave transition even if it is excited by means of two lasers operating in the optical range. The contrast of the dark line is then limited by the relaxation of the coherence between the two sub-states. It can be induced by the collisions of the atoms with the buffer gas and/or the cell glass [13] and by the noise on the relative phase between the optical fields [11, 14].

We investigated in [15] a three-photon CPT which occurs in a four-level atomic system showing a N -shaped laser interaction scheme, where three out of the four involved states are stable or metastable. Extending from two to three lasers involved in the dark resonance condition allows the cancellation of the first order Doppler effect by a geometric phase matching of the three laser wave-vectors [16–20], simulating a Lamb-Dicke effect with an effective infinite wavelength. This example of N -level scheme can be found in the heaviest alkaline-earth ions Ca^+ , Sr^+ and Ba^+ [15] and in alkaline-earth-metal neutral atoms like Sr and Yb [20]. We report here the first observation of a three-photon dark resonance in a cloud of Ca^+ ions, stored in a linear quadrupole trap, and laser-cooled by Doppler laser cooling. In this ion, the three optical fields required to build the coherent dark state lie in the optical and near infra-red domain, spanning more than one octave. Therefore, their phase coherence is insured by an ultra-stable laser through a simultaneous lock on an optical frequency comb (OFC) [21, 22]. The dark resonance condition defines a combination of the three optical frequencies, which is referenced to a magnetic dipole transition at 1.82 THz.

In the following, we first present the experimental conditions for observing a three-photon dark resonance in the fluorescence of a cloud of trapped ions. We review the major effects which contribute to the linewidth, frequency shift and contrast of the dark line as there are the Doppler effect, the Zeeman effect and power-induced

* caroline.champenois@univ-amu.fr

effects.

CONDITION FOR OBSERVATIONS OF A THREE-PHOTON CPT

The three-photon dark line is observed in the laser-induced fluorescence emitted by a cloud of $^{40}\text{Ca}^+$ ions, stored in a linear RF quadrupole trap. The calcium ions are Doppler laser-cooled on their resonance transition $4S_{1/2} \rightarrow 4P_{1/2}$ at 396.85 nm (label *B*). This transition is not closed and once in the excited state $4P_{1/2}$, the ions can decay to the metastable state $3D_{3/2}$ with a probability $\beta = 0.064$ [23]. Keeping the ions within the cooling cycle thus implies a second "repumping" laser, tuned to the dipole transition $3D_{3/2} \rightarrow 4P_{1/2}$ at 866.21 nm (label *R*). The third laser involved in the CPT process is resonant with the electric quadrupole transition $4S_{1/2} \rightarrow 3D_{5/2}$ at 729.15 nm (label *C*, see Fig. 1, **a** for the transition scheme).

Because it is based on the second order expansion of the interaction Hamiltonian, this last transition has a typical coupling strength which is 8 orders of magnitude smaller than the one induced on the dipole transition involved in the laser cooling [24]. Despite of the weakness of the laser-atom interaction on this transition, it can play a major role in the internal state dynamics provided that a resonance condition is fulfilled [15]. By a partial diagonalisation of the system, this condition can be extrapolated from two-photon Λ -scheme dark resonances [1] and it writes

$$\Delta_R = \Delta_B - \Delta_C - \delta_C \quad (1)$$

where $\Delta_R, \Delta_B, \Delta_C$ are the one-photon detunings of the three lasers and δ_C is the light-shift induced by the quadrupole coupling on the 729 nm transition [15] (see appendix). The trapping state is a coherent superposition of the three stable and metastable dressed states that is not coupled by laser excitation and once trapped in this state, the ions do not emit any photon.

When fulfilled, the three-photon resonance condition implies a strong relation between the three laser frequencies

$$\omega_R + \omega_C - \omega_B + \delta_C = \omega_{THz} \quad (2)$$

with ω_{THz} the frequency of the magnetic dipole transition between $3D_{3/2}$ and $3D_{5/2}$, which appears as the reference transition. The frequency ω_{THz} is 1.82 THz in Ca^+ and its absolute value is known with a ± 8 Hz uncertainty through Raman spectroscopy on a single trapped ion [25, 26]. Considering the typical intensity and detuning for the laser at 729 nm, δ_C is below 100 Hz and can be neglected in the results reported in the following.

In the experiments presented here, the three lasers copropagate along the symmetry axis of a linear quadrupole

RF-trap (see Fig. 1, **b**) and the effective wave-vector $\Delta \vec{k}$ controlling the first order Doppler effect on the dark line is the one of the magnetic dipole transition $k_{THz} = 2\pi/\lambda_{THz}$ with λ_{THz} the $3D_{3/2}$ - $3D_{5/2}$ transition wavelength, equal to 165 μm . The quadrupole trap is described in [27, 28], its main characteristics are an inner radius of 3.93 mm for a rod radius of 4.5 mm [29] and an RF trapping frequency of 5.2 MHz. For the work presented here, it is operated with an RF-voltage difference between neighboring rods of 826 V_{pp} (Mathieu parameter $q_x = 0.24$) and a typical cloud contains a few tens to thousands ions. The Doppler-laser cooling drives the ion cloud from a gas, through the liquid, to a crystal phase [30] with a temperature estimated to be of the order of 10 mK. Once in the liquid and crystal phase, the ion cloud forms an ellipsoid [31, 32] with a diameter ranging from 80 to 280 μm and a length ranging from 120 to 740 μm for a number of ions comprised between 40 and 2750 (see Fig. 1, **c**). The 397 nm and 866 nm lasers have an elliptical cross-section, with an aspect ratio of 2 and a mean-squared diameter at the position of the cloud equal to 4.0 mm and 4.7 mm, respectively. The laser intensity and wave-vectors can be considered uniform all over the ion cloud. The 729 nm laser has the smallest size with a waist diameter measured to 300(± 20) μm . It is still larger than the largest of the cloud diameters but its intensity is not uniform over the largest clouds. Keeping all the atoms inside the three laser beams cancels any broadening induced by finite interaction time due to atom motion, which is an identified broadening cause of two-photon CPT lines when observed on an atomic beam or a gas in a cell [7, 33, 34].

For the observation of the dark lines, the three involved lasers are admitted continuously on the cloud. As well-known for the two-photon CPT, the stability of the phase relation between the three dressing lasers is mandatory to reach a stationary dark state. To that purpose, we use a commercial OFC to transfer the phase stability between the three lasers [22]. We take advantage of an ultra stable laser at 729 nm (relative Allan variance of 10^{-14} at 1 s) to serve as a local reference for the offset-free OFC, produced by frequency difference in a non-linear crystal (TOPTICA DFC CORE+). The OFC repetition rate f_{rep} is 80 MHz and three dedicated coherent outputs at 729, 794 and 866 nm allow three simultaneous phase locks (the 397 nm radiation is produced by second harmonic generation). First, the OFC is locked onto the 729 nm laser by a phase-locked loop (PLL) using the beat signal of the ultra stable laser and the closest comb eigen-mode. Then, the 794 and 866 nm lasers are locked onto the OFC by the same technique. Their frequency measurement requires to identify the indexes $N_{B,R,C}$ of their closest eigen-mode emitted by the OFC, and to measure the relative value of the laser frequency compared to this eigen-mode which is bound by $\pm f_{rep}/2$. The indices $N_{B,R,C}$ are determined without ambiguity with the help of a wave-

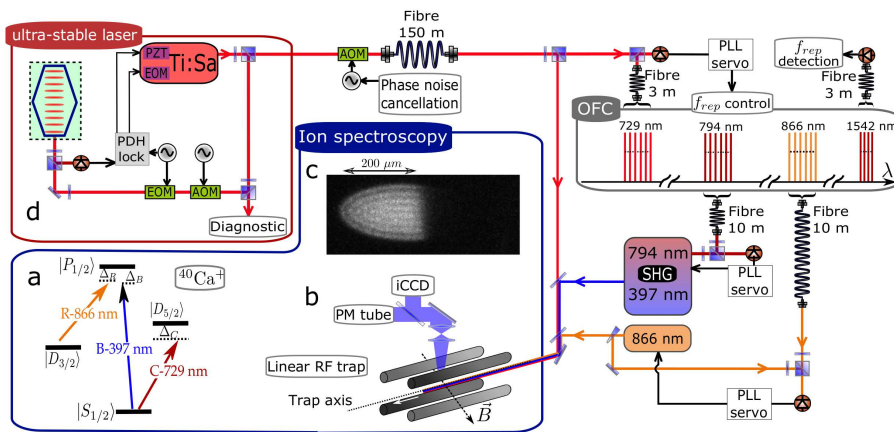


FIG. 1. **a** : Transition scheme for the 3-photon CPT in Ca^+ , **b** : Schematic of the experimental set-up : the three laser beams are propagating along the trap symmetry axis, the linear radio-frequency trap is represented by its four rods, the laser induced fluorescence is recorded on a photomultiplier (PM tube) for photon counting and a intensified CCD camera for spatial resolution of the fluorescence. **c** : picture of a cloud made of $710 (\pm 35)$ ions, the ions shelved in the metastable $D_{5/2}$ state or trapped in the coherent superposition are dark and split from the bright ions because they do not feel the radiation pressure induced by the cooling laser on the bright ions. **d** : set-up for the laser phase-lock, based on an OFC locked onto an ultra-stable Ti:Sa laser. AOM : acousto-optic modulator, EOM : electro-optic modulator, PDH : Pound-Drever-Hall, PLL : phase-lock loop, SHG : second harmonic generation.

meter with an accuracy of ± 10 MHz. The uncertainty on each laser frequency measurement lies in the kHz range and is due to $N_{B,R,C} \times \sigma_{rep}$ with σ_{rep} the uncertainty of the repetition rate equal on average to 1.5 mHz (one standard deviation). The resulting uncertainty on the deduced THz frequency benefits from the combination $(N_B - N_R - N_C) \times \sigma_{rep}$ which is of the order of 34 Hz, two orders of magnitude lower than the optical frequency uncertainty.

Spectra are observed when collecting the photons emitted at 397 nm on the $4P_{1/2} \rightarrow 4S_{1/2}$ transition while the frequency of the R -laser is scanned. Typical laser powers are 10 to 20 mW at 397 nm (P_B), 0.5 to 5 mW at 866 nm (P_R) and 5 to 25 mW at 729 nm (P_C). A complete spectrum width is larger than 100 MHz and figure 2 shows a portion of such a spectrum, selected around the three-photon resonance condition as given by Eq. 1. By comparing the two plots of Fig. 2, showing the fluorescence signal with and without the C -laser exciting the weak transition, one can deduce that some ions are "shelved" in the metastable $D_{5/2}$ state [35], independently of any resonant condition. The narrow features superimposed to the reduced signal (blue line) are the signature of the three-photon CPT. They correspond to the trapping of a fraction of the ions from the cooling cycle to the dark state. With the chosen detection scheme, it is not possible to quantify the number of ions transferred from the metastable state to the dark state. More than half of the ions remain bright and thus are laser-cooled. By sympathetic cooling of the dark atoms [36], the ion cloud remains in a liquid phase throughout the complete fre-

quency scan, even if the radiation pressure is responsible for a spatial separation of the bright and dark ions (see Fig. 1,c). This sympathetic cooling offers the great advantage of keeping constant the number of ions inside the laser beam during the whole recording.

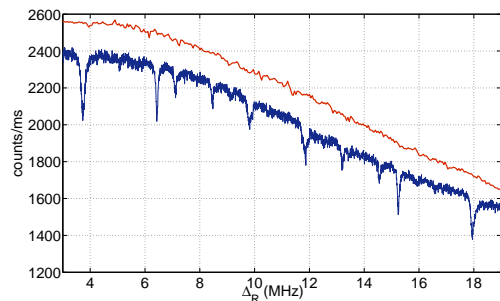


FIG. 2. Laser induced fluorescence of a cloud of laser cooled $560 (\pm 25)$ ions versus the detuning of the repumping R -laser. The top curve shows photon counts when the cooling and repumping lasers are on ($P_B = 10$ mW, $P_R = 1$ mW). For the lower curve, the 729 nm laser is also applied ($P_C = 12.1$ mW). Background : $570 (\pm 25)$ counts/ms

The splitting of the dark line into several pairs of lines is due to the local magnetic field which lifts the degeneracy of the Zeeman sub-states. A magnetic field of the order of 1 Gauss is applied and the three laser polarizations are linear, perpendicular to the trap axis and nearly perpendicular to the local magnetic field. We label each transition by a number m_{THz} according to its Zeeman shift on the THz transition frequency

$\delta_Z(m_{THz}) = m_{THz}\mu_B B$. With $g_{3/2}$ and $g_{5/2}$, the Landé factors of the $D_{3/2}$ and $D_{5/2}$ states, and $m_J(D_{3/2})$ and $m_J(D_{5/2})$ the Zeeman substates involved in the transition, $m_{THz} = g_{5/2}m_J(D_{5/2}) - g_{3/2}m_J(D_{3/2})$. Table I gathers the transitions based on the largest couplings (quantified by their relative Rabi frequencies) imposed by the chosen laser polarization, relative to the local magnetic field and controlled by the selection rules of dipole and quadrupole transitions [37]. The stability of each line

TABLE I. Zeeman sub-states of the two metastable states giving rise to the observed THz transitions. The corresponding THz transitions are labelled by the number m_{THz} , defined by the Zeeman shift $\delta_Z(m_{THz}) = m_{THz}\mu_B B$ (for the labelling only, m_{THz} is rounded in the assumption of a Landé g -factor equal to 2 for the electron). $\bar{\Omega}_C$ and $\bar{\Omega}_R$ are the Rabi frequencies relative to the one of $m_{THz} = \pm 21/5$. All the transitions share the same Rabi frequency on the B -transition.

$m_J(D_{3/2})$	$m_J(D_{5/2})$	m_{THz}	$\bar{\Omega}_C$	$\bar{\Omega}_R$
$\mp 3/2$	$\pm 5/2$	$\pm 21/5$	1	1
$\pm 1/2$	$\pm 5/2$	$\pm 13/5$	1	$1/\sqrt{3}$
$\mp 1/2$	$\pm 3/2$	$\pm 11/5$	$1/\sqrt{5}$	$1/\sqrt{3}$
$\pm 1/2$	$\pm 3/2$	$\pm 7/5$	$1/\sqrt{5}$	$\sqrt{2/3}$
$\pm 3/2$	$\pm 3/2$	$\pm 3/5$	$1/\sqrt{5}$	1

center frequency is limited by the long term fluctuations (> 100 s) of the local magnetic field measured to 0.4 mG (pk-pk). It contributes an uncertainty proportional to m_{THz} and of the order of 1 kHz. The short term fluctuations of the total local magnetic field are measured to 6 mG (pk-pk) and are responsible for a m_{THz} -dependent broadening of the order of 20 kHz (pk-pk). The Doppler effect on the three-photon dark lines is 415 times smaller than the Doppler effect on the optical cooling transition at 397 nm. It broadens the three-photon dark lines by 20 kHz (FWHM) for a sample at 10 mK. On the spectrum of figure 2, the measured linewidths range from 42 kHz to 218 kHz.

DEMONSTRATION OF THE THREE-PHOTON RESONANCE CONDITION

To prove that these extra lines result from the 3-photon process and are referenced to the THz transition, we focus on the dark line defined by $m_{THz} = -13/5$ because of its high contrast. The R -laser frequency ω_R is scanned for different values of ω_C in an interval of 16 MHz, while ω_B is kept constant. The frequency step is 1 kHz and signal is accumulated for 150 ms at each step. Each scan is reproduced 4 times and averaged. Each observed line profile is fitted to a Lorentzian profile and the center of the line ω_R^c is pointed with an uncertainty of the order of 1 kHz (1σ) conditioned by the frequency step

and the signal to noise ratio. The frequency combination $\Delta_{RCB} = \omega_R^c + \omega_C - \omega_B$ is expected to give access to the magnetic dipole transition frequency, once the experimental shifts removed, the Zeeman shift being the largest one identified. As some non-negligible light-induced effects also shift the dark lines, and their dependence with the m_{THz} number is not known, we do not use the average frequency of the $+m_{THz}$ and $-m_{THz}$ line to deduce the unshifted frequency. We rather estimate the local magnetic field by exploiting several multiline spectra as the one of Fig. 2 and adjusting a linear fit of the dark resonance frequencies $\omega_R^c(m_{THz})$ with the m_{THz} values (see Fig. 3 where they are plotted with respect to the transition frequency $\omega_{P_{1/2}D_{3/2}}$ measured in [38]). The

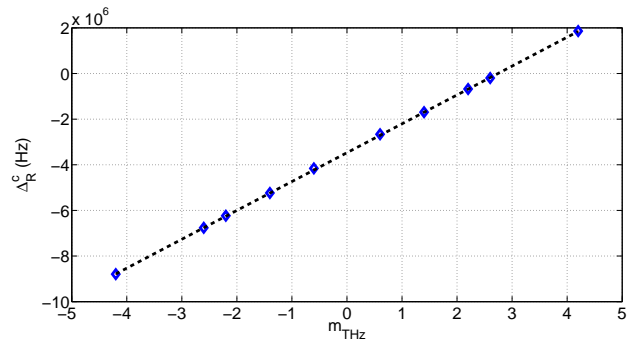


FIG. 3. Dark resonance frequency $\omega_R^c(m_{THz})$ of several Zeeman transition versus their corresponding m_{THz} factor. The frequencies are plotted as detunings $\Delta_R^c(m_{THz})$, see text for details. The black line is the linear fit used to calculate the averaged magnetic field seen by the ions.

Zeeman shift $\delta_Z(-13/5)$ of the $m_{THz} = -13/5$ dark line is evaluated with an uncertainty of ± 6 kHz dominating the total uncertainty of the THz frequency. As shown on Fig 4, the Zeeman corrected transition frequencies do not exactly match the $3D_{3/2}$ to $3D_{5/2}$ transition frequency f_{DD} of reference [26] and are shifted from this reference value by amounts $\delta f = \Delta_{RCB} - \delta_Z(-13/5) - f_{DD}$ which evolve between +5 and -15 (± 6) kHz. These shifts are 3 orders of magnitude smaller than the range covered by the one-photon detuning Δ_R and we consider that the three-photon resonance condition is demonstrated. Nevertheless, their plot against the $m_{THz} = -13/5$ transition detuning $\Delta_R^Z = \omega_R^c - \omega_{P_{1/2}D_{3/2}} + \delta_R^Z(-13/5)$, with $\delta_R^Z(-13/5)$ the Zeeman shift on the R -transition, shows a correlation between the shifts and the detunings that cannot be explained by any drifts in the experimental set-up, neither by the coupling on the quadrupole transition δ_C . Dependence of the light-induced shift with the one-photon detuning is observed in two-photon CPT for a continuous laser excitation [7, 34, 39] and with a Ramsey interrogation scheme [14, 40]. When they are not light-shifts induced by neighbour transitions, they are understood as induced by the relaxation of the coher-

ence between the stable and metastable states involved in the dark state. This relaxation can be due to collisions but most probably to laser relative phase diffusion in our cold atom system in ultra-high vacuum (with a pressure lower than 10^{-9} mbar). In the case of the three-photon CPT, the only light-shifts which can be responsible for a dark line frequency shifts are the one shifting the $3D_{3/2}$ or the $3D_{5/2}$ Zeeman sub-states, as the other ones cancel in the three photon resonance condition (Eq. 1).

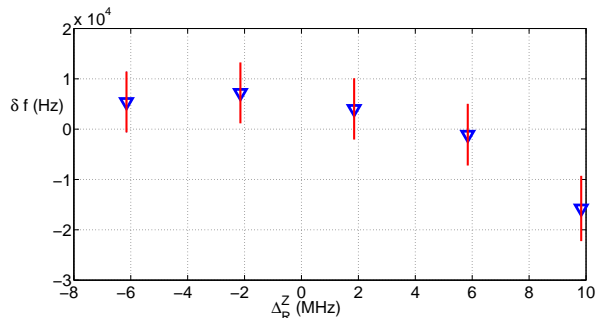


FIG. 4. Frequency shift δf on the 1.82 THz transition, for the $m_{THz} = -13/5$ dark line observed for 5 different sets of $\{\omega_C, \omega_B\}$, versus the one-photon detuning Δ_R^Z that fits the three photon resonance condition. The Zeeman effect is removed from the shift and added to the measured one-photon detuning for the Zeeman shifted R -transition (Eq. 1). Fixed values : $P_B = 10$ mW, $P_R = 2$ mW, $P_C = 8$ mW, $\Delta_B = -24.94$ MHz (errorbar = ± 1 std).

POWER-INDUCED SHIFTS

In the case of a three-photon CPT, interpreted as a laser-mediated Λ -scheme [15], the relevant one-photon detuning is Δ_R and the laser couplings on the two arms of the Λ -scheme are dominated by the laser excitation on the R -transition. This description of the N -level scheme is relevant for a strong enough coupling on the weak C -transition. This is confirmed by results reported on Fig. 5 where, contrary to a conventional light-shift effect, it takes a minimum laser power P_C for the frequency shift to reach a value independent of this power. This behaviour is attributed to an ineffective Λ -scheme when the coupling on the quadrupole transition is too weak.

The dependence of the frequency shift with the power of the R -laser is shown on Fig. 6 for the $m_{THz} = -13/5$ line. The results show a linear behavior of δf with P_R which can be extrapolated for $P_R = 0$ to $6.0(\pm 3.4)$ kHz, showing that other experimental parameters are also responsible for shifts. In the case of the $m_{THz} = -13/5$ line, a light-shift effect can be induced by a small projection of the R -laser polarisation along the magnetic field axis which then couples the $3D_{3/2}$, $m = -1/2$ sub-state to $4P_{1/2}$, $m = -1/2$ sub-state. The light-shift induced

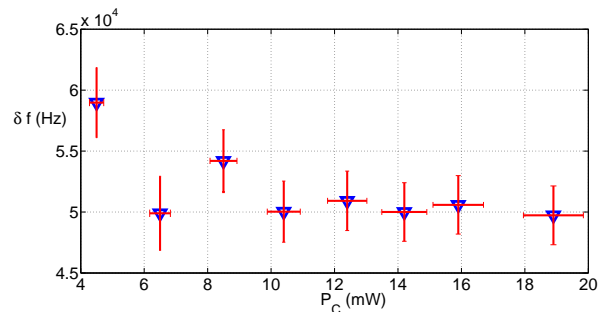


FIG. 5. Frequency shift of the Zeeman sub-transition $m_{THz} = -13/5$ vs P_C , the laser power on the quadrupole transition, for one-photon detuning $\Delta_R^Z = -10.6$ MHz. The other laser powers are $P_B = 10$ mW and $P_R = 1$ mW.

by the far detuned R -couplings to the $4P_{3/2}$ state is estimated to values lower than 10 Hz. In the regime of parameter used to observe the three-photon dark line, no significant dependence of the frequency shifts with the laser power P_B could be observed, for power ranging 5 to 20 mW. Another kind of power-induced shifts have been identified in two-photon CPT-clock [39, 41]. They are due to the relaxation of the coherence between the stable and metastable states involved in the dark state and are proportional to the one-photon detuning. This extra effect is certainly contributing to the total power-induced shift, due to the finite phase coherence of the three lasers [21, 22].

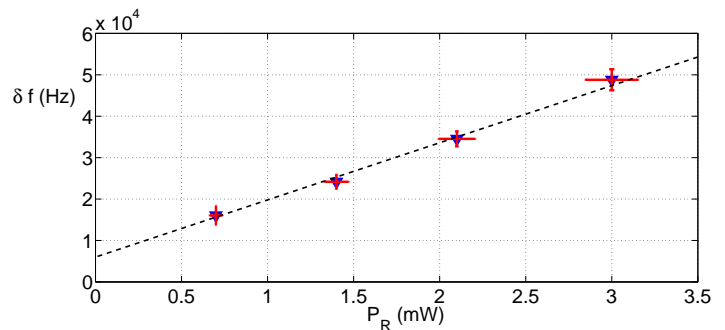


FIG. 6. Frequency shift of the Zeeman sub-transition $m_{THz} = -13/5$ measured for different R -laser power P_R (blue dots) and for an effective one-photon detuning $\Delta_R^Z = -7.74$ MHz. The dark line is a linear fit of this plots, with slope 13.8 ± 1.8 kHz/mW and limit shift for null power P_R equal to 6.0 ± 3.4 kHz (1σ). The other laser powers are $P_B = 19$ mW and $P_C = 10.4$ mW.

METROLOGICAL PERFORMANCES

To quantify the metrological performances of the 3-photon CPT dark line as a THz reference, let's assume these shifts are under control and focus on the linewidth, the absolute signal level as well as the contrast of the dark line. We recall that within the present experimental set-up, each line is broadened by a residual Doppler effect (estimated to a minimum of 20 kHz FWHM) and by a fluctuating Zeeman effect (estimated to $8.4 \times m_{THz}$ kHz pk-pk). Furthermore, in the range of our experimental parameters, the observed power-induced broadening is only due to the coupling on the R -transition. The narrowest observed dark lines (linewidth of 45 kHz for $P_R = 0.7$ mW) are the ones with the smallest coupling on the R -transition, identified by $|m_{THz}| = 11/5$ and $13/5$ (see table I). The maximum dark line contrast, reaching 25%, is observed for the lines $|m_{THz}| = 13/5$ and $21/5$ and they are the ones with the largest coupling on the C -transition. These two independent conditions point $|m_{THz}| = 13/5$ as the transition of the best contrast/broadening compromise in the context of our present experimental set-up.

In Fig. 7, we have plotted the linewidth and contrast of the $m_{THz} = -13/5$ dark line for the five different sets of $\{\omega_C, \omega_B\}$, as observed for Fig. 4. The data show a depen-

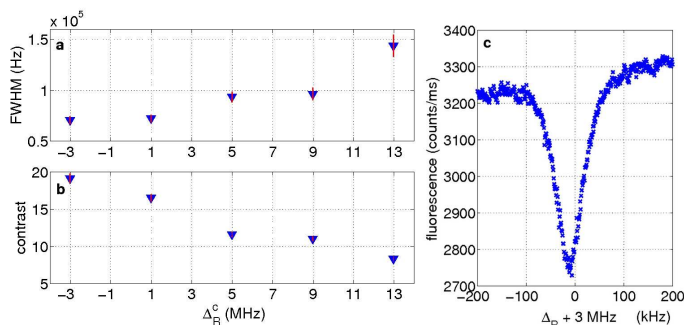


FIG. 7. FWHM (a) and contrast (b) of the $m_{THz} = -13/5$ dark line observed for 5 different sets of $\{\omega_C, \omega_B\}$, vs Δ_R^C , same experiments as for Fig. 4. (c) : line profile of the dark line showing the largest contrast and the smallest linewidth of these 5 observations. The background induced by stray light is 520 ± 25 counts/ms.

dence of the linewidth and contrast with the one-photon detuning Δ_R for which the CPT occurs while all the laser powers are kept constant. We think that this effect can be explained by the relative position of the dark line in the broader fluorescence spectra profiles of the trapped ions, due to a competition with the strong transitions involved in laser cooling. Further studies are required to identify the best condition to reach the contrast/linewidth optimum but these curves open very positive perspectives as we find in the same detuning range the smallest shifts,

the largest contrast and the narrowest linewidth.

Considering that the Doppler broadening can be cancelled by obeying the phase matching condition $\vec{k}_B - \vec{k}_R - \vec{k}_C = \vec{0}$ [18], or alternatively by a Lamb-Dicke effect on the THz-wavelength scale [42], the signal over noise ratio could be increased with a larger number of ions building the dark line. By expanding the size of the cloud, the position dependant systematic shifts are expected to broaden the spectroscopic lines [43–45]. Nevertheless, when varying the number of trapped ions from 60 to 400 ions, with all other parameters fixed, we observe no variation of the THz-frequency shift, neither of the dark line width, within the 6 kHz resolution.

As the magnetic field fluctuations can be actively reduced by a factor 50 and the sensitivity to these fluctuations can also be reduced by using the transitions $m_{THz} = \pm 1/5$ if other laser polarisation and propagation directions are permitted by the set-up, a linewidth in the kHz range, or lower, together with a large contrast, seems to be very accessible. It would enable to identify effects, which are so far too small to be detected and to access a resolution in the 10^{-9} range, which is the state of the art in the THz precision spectroscopy [42, 46]. Indeed, in a system without any experimentally induced decoherence, one can show that sub-kHz linewidths can be observed [18]. Furthermore, with a 25% contrast and an average fluorescence signal of 4000 counts/ms which is the typical value for the fluorescence of one thousand trapped ions in the optimum condition for a narrow dark line, the signal to noise ratio at 1 ms reaches 16. Even with a kHz linewidth, such a large signal to noise ratio allows the resolution to be increased to the 10^{-11} range by averaging data over seconds.

CONCLUSION

The demonstrated 3-photon CPT has a large potential for high-resolution spectroscopy. Very similar to 2-photon CPT, the interrogation protocols depends on numerous parameters that have to be further explored. In 2-photon CPT, they are strongly mitigated by the use of Ramsey-type pulsed protocol [47–49] and using a pulsed interrogation method for the 3-photon CPT is certainly a route to test. The originality of our approach allows to access the THz domain, an insufficiently explored and very promising spectral domain, so far associated to rotational transitions in light molecules. Although the production of a continuous-wave THz radiation from the three involved optical radiations is still an issue, this configuration could be of use to transmit the 1.82 THz reference signal by optical means and to benefit from very efficient detectors. Indeed, because THz radiation hardly propagates along long distances in air, its phase-coherent transfer implies to coherently duplicate its phase information onto an optical carrier [50]. Build-

ing a THz referenced signal from three coherent lasers avoids this duplication stage and allows its transmission over long distances through optical fibers. Independently of the frequency range of the reference transition, the demonstration that a narrow line can be produced in a mesoscopic sample by implementing a Doppler-free technique opens the route to its implementation on a large variety of atomic systems.

This experiment has been financially supported by the Labex FIRST-TF (ANR-10-LABX-48-01), the A*MIDEX project (ANR-11-IDEX-0001-02), EquipEx Refimeve+ (ANR-11-EQPX-0039) all funded by the Investissements d'Avenir French Government program, managed by the French National Research Agency (ANR). Fundings from CNES (contract 151084) and Région PACA are acknowledged. MC acknowledges FIRST-TF for funding and stimulating scientific environment, CyC acknowledges financial support from CNES and Région Provence-Alpes-Cote d'Azur.

Conditions for a three-photon dark resonance

The condition for a three-photon dark resonance implying the weak quadrupole transition in Ca^+ is better explained in the dressed state picture where the system of interest is a motionless atom represented by its quantized internal states plus n_B photons at 397 nm (energy $n_B \times \hbar\omega_B$), n_R photons at 866 nm (energy $n_R \times \hbar\omega_R$) and n_C photons at 729 nm (energy $n_C \times \hbar\omega_C$) (see Fig.1, **a** for the level scheme). The three atom-laser interactions are characterised by their Rabi frequencies $\Omega_B, \Omega_R, \Omega_C$ which are linear with the local laser electric field, whatever the nature of this interaction. The eigenvalues of the non-coupled hamiltonian depend on each laser detuning which are defined like $\Delta_B = \omega_B - \omega_{P_{1/2}S_{1/2}}$, $\Delta_R = \omega_R - \omega_{P_{1/2}D_{3/2}}$, and $\Delta_C = \omega_C - \omega_{D_{5/2}S_{1/2}}$ with $\omega_{P_{1/2}S_{1/2}}$, $\omega_{P_{1/2}D_{3/2}}$ and $\omega_{D_{5/2}S_{1/2}}$ the atomic transition frequencies. Like further explained in [15], the dressed laser-coupled subsystem $\{(S_{1/2}, n_B, n_R, n_C), (D_{5/2}, n_B, n_R, n_C - 1)\}$ can be diagonalised at the lowest order of the perturbation and the new eigenstates $\{|S\rangle, |Q\rangle\}$ are then a coherent superposition of the two uncoupled states. $\{|S\rangle, |Q\rangle\}$ are both coupled to the $|P\rangle$ state ($P_{1/2}, n_B - 1, n_R, n_C$) through the strong dipole transition excited by the 397 nm laser, but with a very different strength, depending on the detuning Δ_C and the Rabi frequency Ω_C , which control the proportion of the two uncoupled states in the new eigenstates. Including $|D\rangle = (D_{3/2}, n_B - 1, n_R + 1, n_C)$, the subsystem $\{|Q\rangle, |P\rangle, |D\rangle\}$, coupled by the two dipole transitions forms a Λ -scheme where the two feet are stable or metastable. This scheme is the paradigm of the configurations giving rise to a coherent population trapping in a dark state when the two (meta)stable states are degenerated in the dressed state picture [1]. Because the

Λ -scheme was built by first diagonalising one of the interactions, this resonance condition implies here not two but three photons and writes

$$\Delta_R = \Delta_B - \Delta_C - \delta_C \quad (3)$$

where δ_C is the light-shift induced by the quadrupole coupling on the 729 nm transition [15]. The laser couplings on the effective Λ -scheme are Ω_R and $\alpha_C \Omega_B$ with $\alpha_C = \Omega_C / 2\Delta_C$ the mixing coefficient induced by the quadrupole coupling.

-
- [1] E. Arimondo (Elsevier, 1996) p. 257.
 - [2] G. Alzetta, A. Gozzini, L. Moi, and G. Orriols, *Il Nuovo Cimento B* (1971-1996) **36**, 5 (1976).
 - [3] O. Schmidt, R. Wynands, Z. Hussein, and D. Meschede, *Phys. Rev. A* **53**, R27 (1996).
 - [4] A. Nagel, L. Graf, A. Naumov, E. Mariotti, V. Biancalana, D. Meschede, and R. Wynands, *Europhysics Letters (EPL)* **44**, 31 (1998).
 - [5] P. D. D. Schwindt, S. Knappe, V. Shah, L. Hollberg, J. Kitching, L.-A. Liew, and J. Moreland, *Applied Physics Letters* **85**, 6409 (2004), <https://doi.org/10.1063/1.1839274>.
 - [6] N. Cyr, M. Tetu, and M. Breton, *IEEE Transactions on Instrumentation and Measurement*, 640 (1993).
 - [7] R. Wynands and A. Nagel, *Applied Physics B* **68**, 1 (1999).
 - [8] J. Vanier, *Applied Physics B* **81**, 421 (2005).
 - [9] P. Yun, F. m. c. Tricot, C. E. Calosso, S. Micalizio, B. François, R. Boudot, S. Guérandel, and E. de Clercq, *Phys. Rev. Applied* **7**, 014018 (2017).
 - [10] M. Abdel Hafiz, G. Coget, P. Yun, S. Guérandel, E. de Clercq, and R. Boudot, *Journal of Applied Physics* **121**, 104903 (2017), <https://doi.org/10.1063/1.4977955>.
 - [11] X. Liu, E. Ivanov, V. I. Yudin, J. Kitching, and E. A. Donley, *Phys. Rev. Applied* **8**, 054001 (2017).
 - [12] R. H. Dicke, *Phys. Rev.* **89**, 472 (1953).
 - [13] J. Kitching, S. Knappe, and L. Hollberg, *Applied Physics Letters* **81**, 553 (2002), <https://doi.org/10.1063/1.1494115>.
 - [14] P. R. Hemmer, M. S. Shahriar, V. D. Natoli, and S. Ezekiel, *J. Opt. Soc. Am. B* **6**, 1519 (1989).
 - [15] C. Champenois, G. Morigi, and J. Eschner, *Phys. Rev. A* **74**, 053404 (2006).
 - [16] G. Grynberg, F. Biraben, M. Bassini, and B. Cagnac, *Phys. Rev. Lett.* **37**, 283 (1976).
 - [17] T. Hong, C. Cramer, W. Nagourney, and E. N. Fortson, *Phys. Rev. Lett.* **94**, 050801 (2005).
 - [18] C. Champenois, G. Hagel, M. Houssin, M. Knoop, C. Zumsteg, and F. Vedel, *Phys. Rev. Lett.* **99**, 013001 (2007).
 - [19] I. I. Ryabtsev, I. I. Beterov, D. B. Tretyakov, V. M. Entin, and E. A. Yakshina, *Phys. Rev. A* **84**, 053409 (2011).
 - [20] D. S. Barker, N. C. Pisenti, B. J. Reschovsky, and G. K. Campbell, *Phys. Rev. A* **93**, 053417 (2016).
 - [21] N. Scharnhorst, J. B. Wübbena, S. Hannig, K. Jakobsen, J. Kramer, I. D. Leroux, and P. O. Schmidt, *Opt. Express* **23**, 19771 (2015).

- [22] M. Collombon, G. Hagel, C. Chatou, D. Guyomarc'h, D. Ferrand, M. Houssin, C. Champenois, and M. Knoop, *Opt. Lett.* **44**, 859 (2019).
- [23] M. Ramm, T. Pruttivarasin, M. Kokish, I. Talukdar, and H. Häffner, *Phys. Rev. Lett.* **111**, 023004 (2013).
- [24] M. Knoop, C. Champenois, G. Hagel, M. Houssin, C. Lisowski, M. Vedel, and F. Vedel, *Eur. Phys. J. D* **29**, 163 (2004).
- [25] R. Yamazaki, H. Sawamura, K. Toyoda, and S. Urabe, *Phys. Rev. A* **77**, 012508 (2008).
- [26] C. Solaro, S. Meyer, K. Fisher, M. V. DePalatis, and M. Drewsen, *Phys. Rev. Lett.* **120**, 253601 (2018).
- [27] C. Champenois, J. Pedregosa-Gutierrez, M. Marciante, D. Guyomarc'h, M. Houssin, and M. Knoop, *AIP Conference Proceedings* **1521**, 210 (2013).
- [28] M. R. Kamsap, J. Pedregosa-Gutierrez, C. Champenois, D. Guyomarc'h, M. Houssin, and M. Knoop, *Phys. Rev. A* **92**, 043416 (2015).
- [29] J. Pedregosa, C. Champenois, M. Houssin, and M. Knoop, *Int. J. Mass Spec.* **290**, 100 (2010).
- [30] M. Drewsen, C. Brodersen, L. Hornekær, J. S. Hangst, and J. P. Schiffer, *Phys. Rev. Lett.* **81**, 2878 (1998).
- [31] L. Turner, *Phys. Fluids* **30**, 3196 (1987).
- [32] L. Hornekær and M. Drewsen, *Phys. Rev. A* **66**, 013412 (2002).
- [33] J. E. Thomas, S. Ezekiel, C. C. Leiby, R. H. Picard, and C. R. Willis, *Opt. Lett.* **6**, 298 (1981).
- [34] S. Brandt, A. Nagel, R. Wynands, and D. Meschede, *Phys. Rev. A* **56**, R1063 (1997).
- [35] W. Nagourney, J. Sandberg, and H. Dehmelt, *Phys. Rev. Lett.* **56**, 2797 (1986).
- [36] D. J. Larson, J. C. Bergquist, J. J. Bollinger, W. M. Itano, and D. J. Wineland, *Phys. Rev. Lett.* **57**, 70 (1986).
- [37] I. Sobelman, *Atomic spectra and radiative transitions* (Springer-Verlag, 1992).
- [38] F. Gebert, Y. Wan, F. Wolf, C. N. Angstmann, J. C. Berengut, and P. O. Schmidt, *Phys. Rev. Lett.* **115**, 053003 (2015).
- [39] T. Zanon-Willette, E. de Clercq, and E. Arimondo, *Phys. Rev. A* **84**, 062502 (2011).
- [40] J. W. Pollock, V. I. Yudin, M. Shuker, M. Y. Basalae, A. V. Taichenachev, X. Liu, J. Kitching, and E. A. Donley, *Phys. Rev. A* **98**, 053424 (2018).
- [41] A. Nagel, S. Brandt, D. Meschede, and R. Wynands, *Europhysics Letters (EPL)* **48**, 385 (1999).
- [42] S. Alighanbari, M. G. Hansen, V. I. Korobov, and S. Schiller, *Nature Physics* **14**, 555 (2018).
- [43] K. Arnold, E. Hajiyev, E. Paez, C. H. Lee, M. D. Barrett, and J. Bollinger, *Phys. Rev. A* **92**, 032108 (2015).
- [44] K. J. Arnold and M. D. Barrett, *Phys. Rev. Lett.* **117**, 160802 (2016).
- [45] J. Keller, T. Burgermeister, D. Kalincev, A. Didier, A. P. Kulosa, T. Nordmann, J. Kiethe, and T. E. Mehlstäubler, *Phys. Rev. A* **99**, 013405 (2019).
- [46] G. Hu, T. Mizuguchi, X. Zhao, T. Minamikawa, T. Mizuno, Y. Yang, C. Li, M. Bai, Z. Zheng, and T. Yasui, *Science Report* **7** (2017), 10.1038/srep42082.
- [47] T. Zanon-Willette, V. I. Yudin, and A. V. Taichenachev, *Phys. Rev. A* **92**, 023416 (2015).
- [48] M. Abdel Hafiz, G. Coget, M. Petersen, C. Rocher, S. Guérandel, T. Zanon-Willette, E. de Clercq, and R. Boudot, *Phys. Rev. Applied* **9**, 064002 (2018).
- [49] M. Abdel Hafiz, G. Coget, M. Petersen, C. Rocher, S. Guérandel, T. Zanon-Willette, E. de Clercq, and R. Boudot, *Phys. Rev. Applied* **9**, 064002 (2018).
- [50] S. Nagano, M. Kumagai, H. Ito, M. Kajita, and Y. Hanado, *Applied Physics Express* **10**, 012502 (2017).